


## Article

# The Electronic Structures and Energies of the Lowest Excited States of the $N_s^0$ , $N_s^+$ , $N_s^-$ and $N_s$ -H Defects in Diamond

Alexander Platonenko <sup>1</sup>, William C. Mackrodt <sup>2,\*</sup> and Roberto Dovesi <sup>3</sup><sup>1</sup> Institute of Solid State Physics, University of Latvia, 8 Kengaraga Street, LV-1063 Riga, Latvia<sup>2</sup> Dipartimento di Chimica, Università di Torino, Via P. Giuria 5, 10125 Torino, Italy<sup>3</sup> Accademia delle Scienze di Torino, Via Accademia delle Scienze 6, 10123 Torino, Italy

\* Correspondence: wcm@st-andrews.ac.uk

**Abstract:** This paper reports the energies and charge and spin distributions of the mono-substituted N defects,  $N_s^0$ ,  $N_s^+$ ,  $N_s^-$  and  $N_s$ -H in diamonds from direct  $\Delta$ -SCF calculations based on Gaussian orbitals within the B3LYP function. These predict that (i)  $N_s^0$ ,  $N_s^+$  and  $N_s^-$  all absorb in the region of the strong optical absorption at 270 nm (4.59 eV) reported by Khan et al., with the individual contributions dependent on the experimental conditions; (ii)  $N_s$ -H, or some other impurity, is responsible for the weak optical peak at 360 nm (3.44 eV); and that  $N_s^+$  is the source of the 520 nm (2.38 eV) absorption. All excitations below the absorption edge of the diamond host are predicted to be excitonic, with substantial re-distributions of charge and spin. The present calculations support the suggestion by Jones et al. that  $N_s^+$  contributes to, and in the absence of  $N_s^0$  is responsible for, the 4.59 eV optical absorption in N-doped diamonds. The semi-conductivity of the N-doped diamond is predicted to rise from a spin-flip thermal excitation of a CN hybrid orbital of the donor band resulting from multiple in-elastic phonon scattering. Calculations of the self-trapped exciton in the vicinity of  $N_s^0$  indicate that it is essentially a local defect consisting of an N and four nn C atoms, and that beyond these the host lattice is essentially a pristine diamond as predicted by Ferrari et al. from the calculated EPR hyperfine constants.

**Keywords:** N-doped diamond; C-centre;  $N_s$  defects; optical spectra;  $\Delta$ -SCF calculations; Gaussian orbitals; B3LYP



**Citation:** Platonenko, A.; Mackrodt, W.C.; Dovesi, R. The Electronic Structures and Energies of the Lowest Excited States of the  $N_s^0$ ,  $N_s^+$ ,  $N_s^-$  and  $N_s$ -H Defects in Diamond. *Materials* **2023**, *16*, 1979. <https://doi.org/10.3390/ma16051979>

Academic Editor: Weiqiu Chen

Received: 26 January 2023

Revised: 21 February 2023

Accepted: 25 February 2023

Published: 28 February 2023



**Copyright:** © 2023 by the authors. Licensee MDPI, Basel, Switzerland. This article is an open access article distributed under the terms and conditions of the Creative Commons Attribution (CC BY) license (<https://creativecommons.org/licenses/by/4.0/>).

## 1. Introduction

The doping of diamond with nitrogen leads to a wide range of substitutional and vacancy-related defects that have been documented extensively (see reference [1] and references therein), including several computational studies of the ground state properties of mono-, di- and higher substitutional systems at various levels of sophistication. Of these, the neutral mono-substituted system,  $N_s^0$ , sometimes referred to as the C-center, has received more attention, with estimates [2,3] of the impurity and unpaired electron levels in the diamond gap and the related semi-conductivity [4], the local lattice structure [5,6], charge and spin distributions [5,6], infra-red and Raman spectra [7,8] and EPR hyperfine constants [5,6]. However, there would appear to be no detailed theoretical accounts of the optical properties, notably the strong absorption at 270 nm (4.59 eV) reported by Chrenko et al. [9], Walker [10], Nazare et al. [11] and more recently by Khan et al. [12] who also found weaker absorptions at 360 nm (3.44 eV) and 520 nm (2.38 eV), whose provenance is less certain than that at 270 nm.

More recently, Jones et al. [13] pointed out that while the P1 signals and 270 nm optical absorption are both identified with the presence of  $N_s^0$ , and used widely to assess its concentration, the CVD grown diamond, for example, shows strong absorption at 270 nm apparently in the absence of, or at greatly reduced concentrations of  $N_s^0$ , at least as indicated by EPR [14]. At typical CVD temperatures of ~1100 K, which is more than

twice the onset temperature of semi-conductivity [14], the concentration of  $N_s^0$  would be expected to be extremely low resulting from the thermal excitation and subsequent dissociation of the resulting bound thermal exciton. This strongly suggests that the zero-spin defect  $N_s^+$ , which results from the ionisation of  $N_s^0$ , might also possess an optical absorption close to 270 nm [15]. It has also been argued [13] that since both natural and synthetic diamonds formed under a range of physical and chemical conditions exhibit optical absorption at 270 nm,  $N_s^-$  and  $N_s\text{-H}$ , which are both EPR inactive, might similarly contribute to the broad absorption in this region.

Previous virtual spectra from several sources [1–3] have provided important information regarding the semi-conductivity in  $N_s^0$ , for they (i) predict a donor/defect band  $\sim 2$  eV below the conduction band edge of the diamond host, which is clearly responsible for the semi-conductivity; (ii) show that the donor band comprises both N and C states [1–3]; and (iii) suggest that the semi-conductivity results from a phonon-driven, thermal transition. However, these spectra are limited in the detail they contain, particularly regarding the thermal transition and optical spectrum. For example, they do not reveal which components of the donor band are responsible for the thermal transition, nor which components of the valence and donor bands lead to the optical absorptions, nor the nature of the hybrid orbitals involved in both. Accordingly, this paper reports direct  $\Delta$ -SCF calculations of the lowest energy excitations of  $N_s^0$ ,  $N_s^+$ ,  $N_s^-$  and  $N_s\text{-H}$  with three primary objectives. The first is to verify, or otherwise, the proposals by Jones et al. [13] concerning the defect states that contribute to the strong 270 nm optical absorption in the N-substituted diamond; the second is to give a detailed description of this and the weaker absorptions at 3.44 eV and 2.38 eV reported by Khan et al. [12]; and the third is to examine in more detail than has hitherto been available, the thermal transition responsible for the semi-conductivity ascribed to  $N_s^0$  [4].

## 2. Materials and Methods

The calculations reported in this study are based on a direct  $\Delta$ -SCF method, as implemented in the CRYSTAL code [16–18], and used previously to describe the lowest energy excitations in the largely ionic systems  $\text{AF}_{\text{II}} \text{NiO}$  [19] and  $\alpha\text{-Al}_2\text{O}_3$  [20], and more recently the highly local GR1 excitation of the neutral diamond vacancy [21] and the self-trapped exciton in diamonds [22], where the method has been described in detail in references [20,22]. The conceptual basis of the approach is that electronic excitation corresponds to the removal of an electron from the ground to a locally excited state that can be treated as a point defect in an otherwise perfect lattice using the long-established super-cell technique. Thus, Wannier–Mott excitons, for example, would be excluded from this approach. The essence of the computational procedure is that it calculates the ground and excited states separately, but identically, from which the difference in energy between the two states is obtained directly from the individual total energies. No restrictions are imposed on the excited state, other than the maintenance of zero occupancy of the donor orbital throughout the SCF procedure, and that electronic structures obtained in this way are fully relaxed to convergence of the total (excited state) energy, with computational conditions and accuracies that are identical to those of the ground state. In terms of the band structures, this corresponds exactly to the difference in energy between the ground and excited states at the  $\Gamma$ -point of the first Brillouin zone, and in terms of the optical spectra, the energy of the direct transition. For systems with indirect gaps, the excitation edge can be calculated from the excited state band structure, but this may not necessarily lie on one of the symmetry directions, and hence is not readily available to the same precision as the  $\Gamma$ -point energy. In principle, the use of a sufficiently large supercell for which the eigenvalues are folded back to the center of the first Brillouin zone ( $\Gamma$ ) could also be examined. However, in the context of the present study, where the *identification* of the optical absorptions is the principal focus, accurate estimates of the excitation edge are not crucial. Since the excited state wavefunction is also obtained, the redistributions of charge and spin are straightforwardly estimated, while the full range of (excited state) dielectric and vibrational properties are also directly calculable.

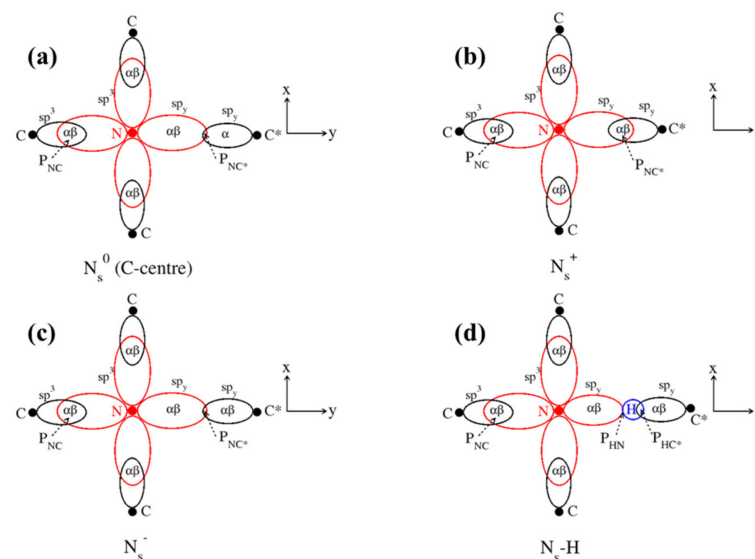
The basis sets and computational conditions used in this paper were identical to those employed in a previous study of the ground-state vibrational properties and EPR constants of  $N_s^0$  [3,23]. As before, the present calculations were based on the hybrid B3LYP functional [24,25] the general utility of which for estimating band gaps in crystalline materials was pointed out by Muscat et al. [26], while more recently, B3LYP has been shown to be superior to PBE0 [27], HSE06 [28] and GGA [29] in direct  $\Delta$ -SCF studies of low-lying excited states in  $AF_{II}$  NiO [19] and the self-trapped exciton in diamond [22]. Modified Pople 6–21G basis sets,  $\{(1s)(2s,2p_x,2p_y,2p_z)(3s,3p_x,3p_y,3p_z)\}$ , were used for C and N, with the exponents of the outer-most sp orbitals set to  $0.23 \text{ Bohr}^{-2}$  and  $0.30 \text{ Bohr}^{-2}$ , respectively, and the truncation of the Coulomb and exchange infinite series controlled by five thresholds  $T_i$  [16], which were set to 8 for ( $T_1$ – $T_4$ ) and 16 for  $T_5$ . The convergence threshold on energy for the self-consistent-field (SCF) procedure was set to  $10^{-8} E_h$  for structural optimizations and to  $10^{-11} E_h$  for the frequency calculations. Supercells containing 64 atoms, and, where necessary, 128 atoms, were used to simulate the defective system, with a shrinking factor of 8 leading to 105 k-points in the IBZ (irreducible Brillouin zone).

As in previous studies of excited states in diamond [21,22], where the (covalent) bonding is described in terms of suitable  $sp^3$  hybrid orbitals that are used directly in the  $\Delta$ -SCF procedure to calculate 1-electron excited state energies and wavefunctions, here, similar C, N and CN hybrid orbitals were constructed from combinations of atomic orbitals such that the sum of the ground state orbital populations, i.e., the total hybrid populations, were  $\sim 1|e|$  and that the local symmetry was preserved. Net atomic charges and bond populations between atoms were obtained from the widely used Mulliken partition of the total charge density (and similarly for the corresponding spin quantities), as discussed in detail by Pascale et al. [30].

### 3. Results

#### 3.1. Ground State

We begin with the ground states both for the information they contain and the essential role they play in the  $\Delta$ -SCF approach to excited states used in this paper. The optimized ground state structures of  $N_s^0$ ,  $N_s^-$  and  $N_s$ -H are locally trigonal about an axis along N and the electron-deficient C atom in  $N_s^0$ ,  $C^*$ , whereas  $N_s^+$  retains the tetragonal symmetry of the host lattice. Two-dimensional stereographic projections of all four systems are shown in Figure 1, where N– $C^*$  is along the y-axis in each case.



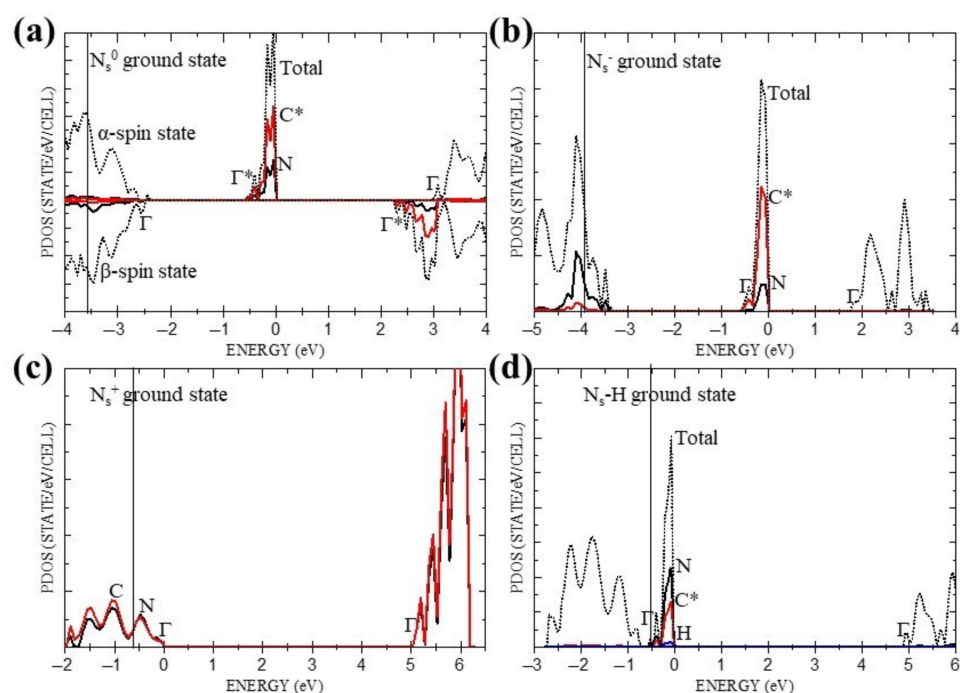
**Figure 1.** Two-dimensional stereographic projections of all four systems: (a)  $N_s^0$ , (b)  $N_s^+$ , (c)  $N_s^-$ , (d)  $N_s$ -H.  $P_{NC/NH}$  indicates bond populations.

Table 1 lists the optimised nearest neighbour (nn) N-C distances ( $\text{\AA}$ ),  $r_{\text{N-C}^*}$ ,  $r_{\text{N-C}}$ , and B3LYP/6-21G atomic charges ( $|e|$ ),  $q_{\text{N}}$ ,  $q_{\text{C}^*}$ ,  $q_{\text{C}}$ , atomic spins ( $|e|$ ),  $s_{\text{N}}$ ,  $s_{\text{C}^*}$ ,  $s_{\text{C}}$ , and overlap charges ( $|e|$ ),  $P_{\text{NC}^*}$ ,  $P_{\text{NC}}$ ,  $P_{\text{HN}}$ ,  $P_{\text{HC}^*}$  in  $\text{N}_s^0$ ,  $\text{N}_s^+$ ,  $\text{N}_s^-$  and  $\text{N}_s\text{-H}$ . The spin of the un-paired electron in  $\text{N}_s^0$ , which is formally located at  $\text{C}^*$ , is predicted to delocalise at N, leading to hyperfine spin-spin interactions with the N nuclear spin, as observed previously [5,6]. In view of the role played by the un-paired electron in the optical spectra, we note that the B3LYP/6-21G prescription used in the present study predicts the Fermi contact term within 2% and the anisotropic dipole-dipole components of the hyperfine coupling tensor to within 11% of the measured values [3]. In all four systems,  $q_{\text{N}}$  is  $\sim -0.5 |e|$ , whereas  $q_{\text{C}^*}$  varies from 0.14  $|e|$  in  $\text{N}_s^0$  and  $\text{N}_s^+$  to  $-0.12 |e|$  in  $\text{N}_s\text{-H}$ . The bond populations,  $P_x$ , are instructive for they confirm the expected bonding between N and C in all four cases ( $P_{\text{NC}} \sim 0.3 |e|$ ) and between N and  $\text{C}^*$  in  $\text{N}_s^+$  ( $P_{\text{NC}^*} \sim 0.2 |e|$ ), with a net anti-bonding N- $\text{C}^*$  interaction predicted in the three trigonal systems ( $P_{\text{NC}^*} < 0$ ). As expected, the present calculations predict a strong covalent bond between H and  $\text{C}^*$  orbitals ( $P_{\text{HC}^*} \sim 0.3 |e|$ ), with H and N non-bonded.

**Table 1.** Optimised (nn) N-C distances ( $\text{\AA}$ ),  $r_{\text{N-C}^*}$ ,  $r_{\text{N-C}}$  and B3LYP atomic charges ( $|e|$ ),  $q_{\text{N}}$ ,  $q_{\text{C}^*}$ ,  $q_{\text{C}}$ , atomic spins ( $|e|$ ),  $s_{\text{N}}$ ,  $s_{\text{C}^*}$ ,  $s_{\text{C}}$ , and overlap charges ( $|e|$ ),  $P_{\text{NC}^*}$ ,  $P_{\text{NC}}$ ,  $P_{\text{HN}}$ ,  $P_{\text{HC}^*}$  in  $\text{N}_s^0$ ,  $\text{N}_s^+$ ,  $\text{N}_s^-$  and  $\text{N}_s\text{-H}$ . Numbers in brackets are the % difference from the diamond C-C distance.

	$\text{N}_s^0$	$\text{N}_s^+$	$\text{N}_s^-$	$\text{N}_s\text{-H}$
$r_{\text{N-C}^*}$	2.05 (+27%)	1.57 (+0.8%)	2.26 (37%)	2.36 (40%)
$r_{\text{N-C}}$	1.50 (−4%)	1.57 (+0.8%)	1.47 (−6%)	1.48 (−5%)
$q_{\text{N}}$	−0.42	−0.42	−0.44	−0.56
$q_{\text{C}^*}$	+0.14	+0.14	−0.05	−0.12
$q_{\text{C}}$	+0.09	+0.14	+0.15	+0.15
$s_{\text{N}}$	0.20 $\alpha$	-	-	-
$s_{\text{C}^*}$	0.76 $\alpha$	-	-	-
$s_{\text{C}}$	0.04 $\beta$	-	-	-
$P_{\text{NC}^*}$	−0.06	+0.20	−0.09	−0.16
$P_{\text{NC}}$	+0.27	+0.20	+0.30	+0.27
$P_{\text{HN}}$	-	-	-	0.0
$P_{\text{HC}^*}$	-	-	-	0.30

We turn now to band structures, for they have been the principal theoretical means for explaining the donor and acceptor levels and related semi-conductivity in  $\text{N}_s^0$ , and providing estimates of the optical spectra [1–3]. Figure 2a–d show the ground-state partial densities of states (PDOS) of  $\text{N}_s^0$ ,  $\text{N}_s^+$ ,  $\text{N}_s^-$  and  $\text{N}_s\text{-H}$ , where the diamond (host) valence band edge is indicated by a solid vertical line and measured from the local virtual band in each case. For  $\text{N}_s^0$ , the  $\alpha$ -band is taken as the majority spin. These indicate that the local states in  $\text{N}_s^+$  are only minimally changed from the host value, whereas  $\text{N}_s^0$ ,  $\text{N}_s^-$  and  $\text{N}_s\text{-H}$  are all predicted to contain a local (filled) defect band,  $\sim 0.6$  eV wide, derived from both N and  $\text{C}^*$  states. However, only  $\text{N}_s^0$  and  $\text{N}_s^-$  with indirect gaps of  $\sim 2.2$  eV and  $\sim 1.8$  eV, are compatible with the reported activation energy for semi-conductivity of  $\sim 1.7$  eV [4].



**Figure 2.** Ground states PDOS for all four systems: (a)  $N_s^0$ , (b)  $N_s^-$ , (c)  $N_s^+$ , (d)  $N_s$ -H. Red solid, black solid, blue solid and black dotted lines correspond to carbon\*, nitrogen, hydrogen and total DOS, respectively. C\* and N refer to Figure 1 and  $\Gamma$  indicates the  $\Gamma$ -points of the individual bands. Vertical solid line indicates a diamond (host) valence band edge.

For completeness, and as a measure of the reliability of the computational methodology used in this study, Table 2 lists the previously reported [19] band gap energies of the host lattice, where  $E_g$  is the calculated un-normalised indirect band gap,  $E_\Gamma$  the lowest direct gap ( $\Gamma_{25'}-\Gamma_{15}$ ), ZPE the zero point energy and  ${}^nE_g$  the normalised gap, ( $E_g$ -ZPE), which was introduced by Cardona et al. [31] to interpret the temperature dependence of the experimental exciton energy gap.

**Table 2.** B3LYP/6-21G band gap energies  $E_g$  and  $E_\Gamma$ , ZPE,  ${}^nE_g$  and  $F_g$  for diamond.

Energy (eV)	Energy (eV)	Observed (eV)
$E_g$	5.76	5.80
$E_\Gamma$ ( $\Gamma_{25'}-\Gamma_{15}$ )	7.00	~7-7.4
ZPE	0.37	0.37
${}^nE_g$	5.39	5.48

Table 3 lists the calculated spin-allowed ( $\Delta s_z = 0$ ) and spin-forbidden ( $\Delta s_z \neq 0$ ) band gaps (virtual transition energies) for  $N_s^0$ , where the indirect and direct  $\alpha \rightarrow \alpha$  transitions are potential candidates for the weak absorptions at 2.38 eV and 3.44 eV, respectively, and the direct ( $\Gamma$ - $\Gamma$ )  $\beta \rightarrow \beta$  transition a candidate for the strong 4.59 eV optical absorption, while the spin-forbidden indirect  $\alpha \rightarrow \beta$  transition can be identified with the activation energy for the thermal (phonon-mediated) semi-conductivity.

Table 4 lists the predicted gaps in  $N_s^+$ ,  $N_s^-$  and  $N_s$ -H, from which  $E_g$  in  $N_s^-$  is in the vicinity of the thermal activation energy of ~1.7 eV, and two indirect transitions in  $N_s$ -H possible contributors to the strong optical transition.

**Table 3.** B3LYP/6-21G spin-allowed ( $\Delta s_z = 0$ ) and spin-forbidden ( $\Delta s_z \neq 0$ ) virtual transition energies in  $N_s^0$  taken from Figure 2a, where the defect ( $N/C^*$ ) band width is 0.53 eV and the gap to the valence band upper edge, 1.9 eV.

Transition	Type	(eV)
$\alpha \rightarrow \alpha$	indirect	3.02
$\alpha \rightarrow \alpha$	direct	3.55
$\beta \rightarrow \beta$	direct	4.60
$\alpha \rightarrow \beta$	indirect	2.22
$\alpha \rightarrow \beta$	direct	2.75
$\beta \rightarrow \alpha$	indirect	5.40
$\beta \rightarrow \alpha$	direct	5.47

**Table 4.** B3LYP/6-21G band gaps in  $N_s^+$ ,  $N_s^-$  and  $N_s$ -H taken from Figure 2b–d where the spin-allowed and spin-forbidden transitions have identical energies.

Gap	$N_s^+$		$N_s^-$		$N_s$ -H	
	Type	(eV)	Type	(eV)	Type	(eV)
$E_\Gamma$	direct	5.09	direct	2.55	direct	5.56
$E_g$			indirect	1.81	indirect	4.86
					indirect	4.99
					indirect	5.43

### 3.2. Excited States

Starting with  $N_s^0$ , Figure 2a indicates that there are three bands from which low-energy excitations originate. They are the  $\alpha$ -spin donor band which, strictly speaking, is part of the  $\alpha$  valence band but for clarity is considered separately from the remainder of the band, which we refer to as the  $\alpha$  valence band, and then the other part is the  $\beta$  valence band. In addition to the two criteria referred to in Section 2 which determine the choice of suitable hybrid orbitals to be used directly in the  $\Delta$ -SCF procedure, in the case of the donor band there is further restriction, namely, that the PDOS shown in Figure 2a requires the ratio of the  $C^*$  to  $N$  orbital densities in the ground state to be  $\sim 3$ . This restricts the choice to a single hybrid namely,  $\{N(2s) + C^*(2p_y) + C^*(3p_y)\}$  which we write more simply as  $N(2s)C^*(2p_y, 3p_y)$ , as shown in Table 5, together with the predicted  $\Gamma$ -point energy,  $\Delta_{SCF}$ , absorption edge,  $E_g$ , and changes in atomic charges,  $\delta q_N$ ,  $\delta q_{C^*}$ ,  $\delta q_C$  and spins  $\delta s_N$ ,  $\delta s_{C^*}$ ,  $\delta s_C$ , resulting from the transition. In the context of the present study, which is concerned with the absorption spectra, the term ‘absorption edge’ is preferred to ‘band gap’ for excited states. Unlike the diamond host, where the dispersion of the lowest unoccupied band is  $\sim 1.6$  eV between the  $\Gamma$ -point ( $\Gamma_{15}$ ) and the minimum energy close to  $\Delta_1$ , the corresponding bands in  $N_s^0$ ,  $N_s^+$ ,  $N_s^-$  and  $N_s$ -H are appreciably flatter, with dispersion energies ranging from 0.04 eV for  $N_s^0$  to 0.16 eV  $N_s^-$ . Thus, for a good approximation, indirect absorption edges,  $E_g$ , are given by the directly calculated energy ( $\Delta_{SCF}$ ) minus the band width, with no ZPE corrections. The full list of directly calculated hybrid excitation energies below the strong absorption edge of the diamond host ( $\sim 5.5$  eV), together with the corresponding changes in atomic charge and spin at the  $N$  and nearest neighbour  $C$  sites, are collected in Table 5. Similarly, the energies of the possible hybrid excitations and changes in local charge and spin for  $N_s^+$ ,  $N_s^-$  and  $N_s$ -H are collected in Tables 6–8.

**Table 5.**  $N_s^0$  B3LYP/6-21G  $\Gamma$ -point gap ( $E_\Gamma$ ), direct SCF ( $\Delta_{SCF}$ ) and absorption edge ( $E_g$ ) energies (eV) and changes to atomic charges ( $|e|$ ),  $\delta q_N$ ,  $\delta q_{C^*}$ ,  $\delta q_C$ , atomic spins ( $|e|$ ),  $\delta s_N$ ,  $\delta s_{C^*}$ ,  $\delta s_C$ , in  $N_s^0$ . t denotes a thermally excited state.  $\alpha$  and  $\beta$  refer to changes in spin-up and spin-down orbitals charges and spins, respectively.

Transition	Type	$E_\Gamma$	$\Delta_{SCF}$	$E_g$	$\delta q_N$	$\delta q_{C^*}$	$\delta_C$	$\delta s_N$	$\delta s_{C^*}$	$\delta s_C$
Donor band										
$\alpha \rightarrow \beta$	N(2s)C*(2p <sub>y</sub> ,3p <sub>y</sub> )	2.75	1.96	1.43	+0.27	−0.16	−0.08	−0.09 $\alpha$	1.86 $\beta$	0.04 $\beta$
	N(2s)C*(2p <sub>y</sub> ,3p <sub>y</sub> )t		1.88	1.35	+0.01	+0.02	0.0	−0.01 $\alpha$	0.01 $\beta$	0.0
Valence bands										
$\alpha \rightarrow \alpha$	N(3s,3p <sub>y</sub> )	3.62	4.23	3.67	−0.78	+0.11	+0.25	1.01 $\beta$	0.08 $\alpha$	0.28 $\alpha$
$\beta \rightarrow \beta$	N(3s,2p <sub>y</sub> )	4.60	4.72	-	−0.55	+0.12	+0.18	1.46 $\alpha$	1.14 $\alpha$	0.27 $\beta$
	N(3s,3p <sub>y</sub> )		3.04	-	−0.80	+0.27	+0.24	1.48 $\alpha$	1.53 $\alpha$	0.30 $\beta$
$\alpha \rightarrow \beta$	N(3s,2p <sub>y</sub> )	2.75	4.72	4.15	−0.55	+0.12	+0.18	1.46 $\beta$	1.14 $\beta$	0.27 $\alpha$
	N(3s,3p <sub>y</sub> )		3.04	2.46	−0.80	+0.27	+0.24	1.48 $\beta$	1.53 $\beta$	0.30 $\alpha$
	C*(3s,2p <sub>y</sub> )		1.00 #	-	−0.01	−0.31	0.0	0.32 $\beta$	2.00 $\beta$	0.02 $\alpha$
	C*(2s,2p <sub>y</sub> ,3p <sub>y</sub> )		1.54	-	+0.04	+0.07	0.0	0.25 $\beta$	1.67 $\beta$	0.01 $\alpha$

# charge transfer to the 3 C atoms nn to C\*.

**Table 6.**  $N_s^+$  B3LYP/6-21G  $\Gamma$ -point gap ( $E_g/E_\Gamma$ ) and direct SCF energy ( $\Delta_{SCF}$ ) (eV) and changes to atomic charges ( $|e|$ ),  $\delta q_N$ ,  $\delta q_{C^*}$ ,  $\delta q_C$ , atomic spins ( $|e|$ ),  $\delta s_N$ ,  $\delta s_{C^*}$ ,  $\delta s_C$ , in  $N_s^+$ .  $\alpha$  and  $\beta$  refer to changes in spin-up and spin-down orbitals charges and spins, respectively.

Transition	$E_g/\Gamma$	$\Delta_{SCF}$	$\delta q_N$	$\delta q_{C^*}$	$\delta_C$	$\delta s_N$	$\delta s_{C^*}$	$\delta s_C$
N(3s,2p <sub>y</sub> )	5.09	5.16	−0.44	+0.13	+0.14	0.97 $\beta$	0.40 $\alpha$	0.21 $\alpha$
N(3s,3p <sub>y</sub> )		2.34	−0.77	+0.33	+0.20	1.00 $\beta$	0.41 $\alpha$	0.23 $\alpha$
C*(2s,3s,2p <sub>y</sub> ,3p <sub>y</sub> )		4.66	+0.17	−0.65	−0.01	0.44 $\alpha$	1.29 $\beta$	0.02 $\beta$
C*(2s,3s,2p <sub>y</sub> )		4.17 #	+0.01	−0.38	−0.01	0.21 $\alpha$	0.94 $\beta$	0.02 $\beta$
C*(3s,2p <sub>y</sub> ,3p <sub>y</sub> )		2.51	+0.16	−0.53	−0.01	0.38 $\alpha$	0.93 $\beta$	0.02 $\beta$

# charge transfer to the 3 C atoms nn to C\*.

**Table 7.**  $N_s^-$  B3LYP/6-21G  $\Gamma$ -point gap ( $E_g/E_\Gamma$ ) and direct SCF energy ( $\Delta_{SCF}$ ) (eV) and changes to atomic charges ( $|e|$ ),  $\delta q_N$ ,  $\delta q_{C^*}$ ,  $\delta q_C$ , atomic spins ( $|e|$ ),  $\delta s_N$ ,  $\delta s_{C^*}$ ,  $\delta s_C$ , in  $N_s^-$ .  $\alpha$  and  $\beta$  refer to changes in spin-up and spin-down orbitals charges and spins, respectively.

Transition	$E_g/\Gamma$	$\Delta_{SCF}$	$E_g$	$\delta q_N$	$\delta q_{C^*}$	$\delta_C$	$\delta s_N$	$\delta s_{C^*}$	$\delta s_C$
N(3s,3p <sub>y</sub> )	2.55	3.94	3.36	−0.77	0.09	0.25	1.03 $\beta$	0.01 $\alpha$	0.28 $\alpha$
C*(3s,2p <sub>y</sub> ,3p <sub>y</sub> )		3.13 #	2.55	0.05	−0.68	0.01	0.0	1.14 $\beta$	0.01 $\alpha$
C*(2s,3s,2p <sub>y</sub> )		4.34 <sup>C</sup>	-	-	-	-	-	-	-
C*(2s,2p <sub>y</sub> ,3p <sub>y</sub> )		3.28 <sup>C</sup>	-	-	-	-	-	-	-

<sup>C</sup>—conducting state; # charge transfer to the 3 C atoms nn to C\*.

**Table 8.**  $N_s$ -H B3LYP/6-21G  $\Gamma$ -point gap ( $E_g/E_\Gamma$ ) and direct SCF energy ( $\Delta_{SCF}$ ) (eV), and changes to atomic charges ( $|e|$ ),  $\delta q_H$ ,  $\delta q_{C^*}$ ,  $\delta q_C$ , atomic spins ( $|e|$ ),  $\delta s_H$ ,  $\delta s_{C^*}$ ,  $\delta s_C$ , in  $N_s$ -H.  $\alpha$  and  $\beta$  refer to changes in spin-up and spin-down orbitals charges and spins, respectively.

Transition	$E_\Gamma$	$\Delta_{SCF}$	$E_g$	$\delta q_N$	$\delta q_{C^*}$	$\delta q_H$	$\delta s_H$	$\delta s_{C^*}$	$\delta s_H$
C*(2p <sub>y</sub> ,3s,3p <sub>y</sub> )	5.56	4.32 #	3.75	−0.03	−0.70	0.44	0.01 $\alpha$	0.40 $\beta$	0.57 $\alpha$

# charge transfer to the 3 C atoms nn to C\*.

#### 4. Discussion

The optimised local ground state structure of  $N_s^0$  is predicted to have  $C_{3v}$  symmetry about the N-C\* direction, in agreement with deductions from the EPR data and previous calculations [3].  $N_s^-$  and  $N_s\text{-H}$ , which have one more electron but no net spin, are also predicted to possess a similar local trigonal symmetry, while  $N_s^+$  with eight valence electrons associated with the inner quintet of atoms, has local  $T_d$  symmetry, as expected. As in previous studies [2,3], the ground state PDOS, shown in Figure 2a–d, and related virtual spectra provide a useful initial assessment of the possible thermal and optical excitations. Thus, as Table 3 indicates, the direct  $\alpha \rightarrow \alpha$  and  $\beta \rightarrow \beta$  excitations of  $N_s^0$  with energies of 3.62 eV and 4.60 eV, respectively, are seen to be consistent with the reported weak and strong optical absorptions at 3.44 eV and 4.59 eV [12]; while the direct and indirect  $\alpha \rightarrow \beta$  energies of 2.75 eV and 2.22 eV are also consistent with the weak optical absorption at 2.38 eV [12], and previously reported peak at  $\sim 2.3$  eV in the photo-conduction spectra [4], and the activation energy for semi-conductivity of  $\sim 1.7$  eV [4]. On the other hand, the virtual spectra of  $N_s^+$ ,  $N_s^-$  and  $N_s\text{-H}$  shown in Table 4 suggest negligible contributions to the reported optical absorption from these systems, apart from  $N_s^-$  which may participate in the weak optical absorption at 2.38 eV [12] and the semi-conductivity in N-doped diamonds. However, as useful as it is, this description is incomplete, for it lacks specific details of the atoms and orbitals involved in the excitations cited.

Turning now to direct  $\Delta$ -SCF calculations, and starting with the donor band in  $N_s^0$ , these find the only excitation below the strong absorption edge of the diamond host to be an  $\alpha \rightarrow \beta$   $\{N(2s)C^*(2p_y, 3p_y)\}$  excitation with a  $\Gamma$ -point energy,  $\Delta_{SCF}$ , of 1.96 eV, as reported in Table 5. This is 0.79 eV lower than that obtained from the virtual spectrum. With reference to Figure 2a, the associated absorption edge,  $E_g$ , corresponds to an excitation from the donor band maximum leading to a value of 1.43 eV, with the absorption peak in the interval (1.43–1.96) eV, which follows from the zero densities of states at donor band extrema. Since this is a spin-flip excitation ( $\Delta S_z \neq 0$ ), the optical intensity is expected to be extremely low as the observed absorption spectrum indicates [12]. Regarding the ‘activation energy’ for semi-conductivity in  $N_s^0$ , which is widely attributed to the thermal excitation of the donor band, it is important to recognize that this is an average energy for conduction over a range of temperatures, with an onset at  $\sim 500$  K ( $\sim 0.04$  eV) [4]. As such, it results from multiple inelastic phonon scattering events with a net energy transfer that is approximately the energy of the thermally excited state of the  $\{N(2s)C^*(2p_y, 3p_y)\}$  hybrid, which is written in Table 5 as  $\{N(2s)C^*(2p_y, 3p_y)\}t$ . Thus, the weak absorption at 2.38 eV [12] might be associated with the optical excitation of a  $\{N(2s)C^*(2p_y, 3p_y)\}$  hybrid, and the ‘activation energy’ for semi-conductivity to the corresponding thermal excitation. Mulliken analysis of the optical excited state wavefunction indicates that the transition involves a *net* transfer of charge ( $\delta q_N$ ) of  $\sim 0.3$  ( $|e|$ ) from N to C\* and the three nn C atoms together with a re-distribution of spin ( $\delta s$ ) resulting from a back donation of charge. The italicised values in Table 5, which correspond to the differences between the optically and thermally excited states, show that further re-distributions of charge and spin in the thermally excited state are negligible.

$\Delta$ -SCF calculations find two possible hybrid excitations from the valence bands in  $N_s^0$  to which the optical absorptions at 4.59 eV and 3.44 eV [12] can be attributed. They are the  $\beta \rightarrow \beta$  and  $\alpha \rightarrow \beta$   $N(3s, 2p_y)$  and  $N(3s, 3p_y)$  excitations, with  $\Gamma$ -point energies of 4.72 eV and 3.04 eV respectively. Furthermore, the  $\alpha \rightarrow \alpha$   $N(3s, 3p_y)$  excitation, for which the absorption edge and  $\Gamma$ -point energies are 3.67 eV and 4.23 eV respectively, cannot be discounted from contributing to the strong absorption at 4.59 eV, for the width of the observed absorption reported by Khan et al. [12] is  $\sim 0.5$  eV, while both Nazare and Neves [11] and Tallaire et al. [14] have observed absorption from  $\sim 4.1$  eV to  $\sim 4.7$  eV in this region as noted previously by Jones et al. [13]. Mulliken analyses of the excited state wavefunctions indicate that all five excitations lead to a net charge transfer from N to the four nn C atoms, including C\*, ranging from  $-0.55$  ( $|e|$ ) to  $-0.80$  ( $|e|$ ) for the  $N(3s, 2p_y)$  and  $N(3s, 3p_y)$  excitations, respectively. Again, there is an appreciable re-distribution of spin resulting from the charge-compensating back donation of charge to the N. There are also



two possible  $\alpha \rightarrow \beta$   $C^*$  hybrid excitations, namely,  $C^*(3s,2p_y)$  and  $C^*(2s,2p_y,3p_y)$  which have not been reported, and in any event will be weak. The first is an excitation from  $C^*$  to its three nn C atoms, which is not shown in Table 5; the second is a pure spin flip with no charge transfer, but simply a re-distribution of spin.

In contrast to the ground state virtual spectrum of  $N_s^+$  shown in Figure 2b which contains a direct absorption edge close to 5 eV,  $\Delta$ -SCF calculations predict several N and  $C^*$  hybrid excitations which are listed in Table 6, but which carry an important caveat. It is the assumption that the uniform negative field used to stabilize the Madelung potential, leads to identical shifts in the total energies of the ground and excited states, despite the re-distribution of charge in the excited state. While this is a reasonable assumption, it remains without proof. The hybrid criteria outlined previously lead to two possible N excitations below the host absorption edge. They are  $N(3s,2p_y)$  and  $N(3s,3p_y)$ , with direct energies of 5.16 eV and 2.34 eV, respectively, which compare with values of 4.23/4.72 eV and 3.04 eV for the corresponding excitations in  $N_s^0$ . In addition, there are three possible  $C^*$  excitations,  $C^*(2s,3s,2p_y,3p_y)$ ,  $C^*(2s,3s,2p_y)$  and  $C^*(3s,2p_y,3p_y)$ , with energies of 4.66 eV, 4.17 eV and 2.51 eV, respectively. Mulliken analyses of the excited state wavefunctions collected in Table 6, indicate that the two N excitations lead to charge transfers to its four equivalent nn C atoms (including  $C^*$ ), whereas the  $C^*$  excitations lead to charge transfers to both N and its three nn C atoms. For all five excitations, there are appreciable re-distributions of spin resulting from back donations of charge. The  $C^*(2s,3s,2p_y,3p_y)$  and  $C^*(2s,3s,2p_y)$  are particularly significant for they support the proposal by Jones et al. [13] that  $N_s^+$  is the likely source of the  $\sim 4.6$  eV optical absorption in circumstances when the concentration of  $N_s^0$  is either extremely low, or absent altogether [14,15]. Furthermore, the present calculations predict that the weak absorption at  $\sim 2.4$  eV in similar circumstances can also be attributed, in part, to  $N_s^+$ .

The ground state PDOS of  $N_s^-$  shown Figure 2c suggests a single low energy excitation with an absorption edge at 1.81 eV and  $\Gamma$ -point energy at 2.55 eV, which can plausibly be attributed to the weak  $\sim 2.4$  eV peak in the optical [12] spectrum. As in the case of both  $N_s^0$  and  $N_s^+$ ,  $\Delta$ -SCF calculations listed in Table 7 posit a greater number of possible excitations, with four below the diamond edge, of which two are predicted to lead to conducting states. Of the remaining two, the  $N(3s,3p_y)$  excitation could contribute to the weak 3.44 eV optical peak [12], at least on energy grounds, for the absorption peak is expected to lie in the interval 3.36 eV–3.94 eV. Similarly, the  $C^*(3s,2p_y,3p_y)$  excitation might contribute to the optical [12] peaks at  $\sim 2.4$  eV. Both excitations involve strong charge transfer, with net depletions of 0.77 ( $|e|$ ) and 0.68 ( $|e|$ ) to their respective nn C atoms. However, the caveat regarding the effect of the uniform electric field once again applies. It is important to emphasise that the calculations reported here for  $N_s^+$  and  $N_s^-$  cannot predict the presence of these defects in N-substituted diamond, but simply their excitation energies and possible contributions to the optical spectrum if there are grounds for inferring their presence [12,13].

Jones et al. [13] and Khan et al. [12] have surmised that under suitable conditions, N-substituted diamond might contain  $N_s$ -H defects, which could make a contribution to the optical spectra. For completeness, therefore, we have examined their low-energy excitations in relation to the reported optical spectrum of N-substituted diamond. B3LYP calculations find  $N_s$ -H to be a wide band gap insulator, as shown in Figure 2d, where the direct and indirect gaps are listed in Table 4. This contains two indirect gaps at 4.45 eV and 4.63 eV, which could reasonably be associated with the  $\sim 4.6$  eV optical absorption [12].  $\Delta$ -SCF calculations given in Table 8 suggest otherwise, with a predicted peak between 3.75 eV and 4.32 eV for the sole excitation,  $C^*(2p_y,3s,3p_y)$ , below the diamond edge. As Table 8 indicates, this involves a transfer of charge from  $C^*$  to H and its three nn C atoms.

A clearer perspective of the  $\Delta$ -SCF energies is shown in Figure 3, where the  $\Gamma$ -point energies for  $N_s^0$  (black),  $N_s^+$  (red),  $N_s^-$  (blue) and  $N_s$ -H (green) are compared with the optical spectra reported by Khan et al. [12]. For clarity, the hybrid designations of the individual  $\Gamma$ -point energies are not included but are readily found in the text. Three significant points emerge from Figure 3. The first is that  $N_s^0$  and its two singly ionised states,

$N_s^+$  and  $N_s^-$  are predicted to absorb in the region of 4.6 eV, with the exact contributions depending on the experimental conditions. The spectra shown in Figure 3 were obtained at  $\sim 800$  K [12], well above the onset temperature of  $\sim 450$  K for semi-conductivity [4], in which case the samples would reasonably be expected to contain both  $N_s^0$  (black) and  $N_s^+$  (red). Under conditions which favour the formation of  $N_s^-$  (blue), calculations suggest that it, too, would contribute to the strong absorption. Second, Figure 3 shows that the very weak absorption at  $\sim 400$  nm, notably in the Sample 2 spectrum, might be attributed to  $N_s^0$  (black),  $N_s^-$  (blue) and  $N_s\text{-H}$  (green), although the predicted absence of  $N_s^+$  (red) suggests  $N_s\text{-H}$ , or some other impurity, as the likely candidate, with the intensities of the  $N_s^0$  and  $N_s^-$  excitations too weak for detection. Third, the optical absorption at  $\sim 500$  nm ( $\sim 2.4$  eV) is attributed to the  $\{N3s,3p_y\}$  and  $C^*(3s,2p_y,3p_y)$  excitations of  $N_s^+$  for exactly the same reason it contributes to the 270 nm ( $\sim 4.6$  eV) absorption, with the  $\alpha \rightarrow \beta$   $\{N(2s)C^*(2p_y,3p_y)\}$  excitation of the donor band again too weak for detection.

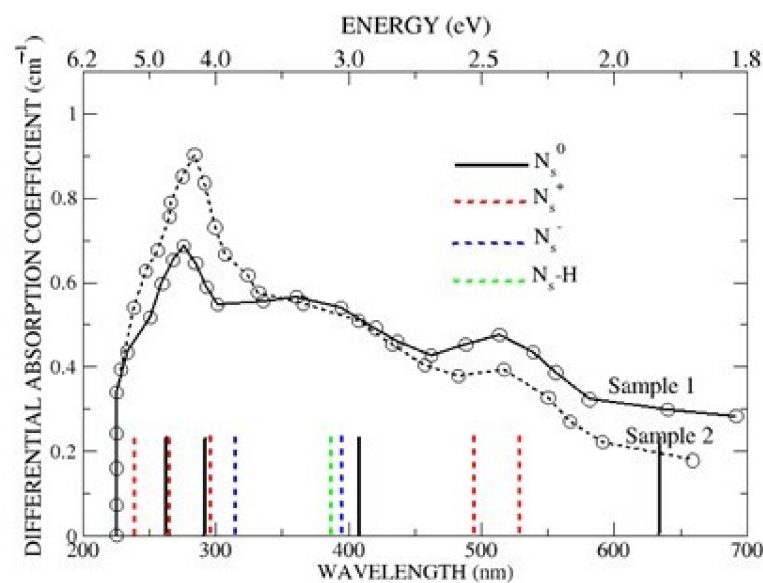


**Figure 3.** Comparison of the predicted  $\Delta$ -SCF  $\Gamma$ -point excitation energies in  $N_s^0$  (black),  $N_s^+$  (red),  $N_s^-$  (blue) and  $N_s\text{-H}$  (green) with the optical spectra reported in Figure 4, Khan et al. [12]. (The heights of the vertical lines are arbitrary).

Finally, we consider briefly a generic issue related to point defects in solids generally, but here, related specifically to  $N_s^0$ . It concerns the extent of the perturbation to the host lattice. The observed EPR hyperfine coupling constants and previous B3LYP calculations by Ferrari et al. [3] find values of  $A_{\text{iso}}$  and  $B_{1,2,3}$  for C atoms beyond nearest neighbour (nn) to N to be 5%, and less, than those at  $C^*$ , which suggests that  $N_s^0$  can properly be described as a local defect consisting of N and four nn C atoms.  $\Delta$ -SCF calculations of the exciton energy ( $\Delta E_{\text{SCF}}$ ) confirm this with values of 7.33 eV for the nn C atoms (Shell 1), 7.22 eV for C atoms once removed (Shell 2) and 7.24 eV, which is the bulk value, thereafter. Thus, for closed shell systems, the calculated exciton energy at different atomic sites from a defect might provide a useful measure of its spatial extent.

## 5. Conclusions

The principal conclusion of this study is that it confirms previous reports that the direct  $\Delta$ -SCF approach to excited states provides information about excited states that is not readily available by other means. More specific conclusions are that,

- The semi-conductivity in N-doped diamond, with an onset at  $\sim 500$  K ( $\sim 0.04$  eV) [4] and activation energy of  $\sim 1.7$  eV [4], results from multiple inelastic phonon scattering

events with a net energy transfer that is approximately the energy of the thermally excited state of the  $\{N(2s)C^*(2p_y, 3p_y)\}$  hybrid of the donor band.

- $N_s^0$  and its first two ionised states,  $N_s^+$  and  $N_s^-$  all absorb optically in the region of 4.6 eV (270 nm), with the contributions from the ionised states dependent on the experimental conditions. Thus, direct  $\Delta$ -SCF calculations support the important suggestion by Jones et al. that  $N_s^+$  contributes to, and in the absence of  $N_s^0$  is responsible for, the 4.59 eV optical absorption in N-doped diamond.
- $N_s$ -H or some other impurity is responsible for the weak optical absorption reported by Khan et al. [12].
- $N_s^+$  is the source of the weak absorption at  $\sim 2.4$  eV (520 nm) for the same reason it contributes to the 4.6 eV (270 nm) absorption.
- The predicted energies of the self-trapped exciton close to  $N_s^0$  confirm previous calculations of Ferrari et al. [3] that it is essentially a local defect consisting of a N and four nn C atoms and that beyond these the host lattice is an essential pristine diamond.

**Author Contributions:** Conceptualization, W.C.M.; methodology, W.C.M.; software, A.P. and R.D.; validation, W.C.M. and A.P.; formal analysis, W.C.M. and A.P.; investigation, A.P., W.C.M. and R.D.; resources, A.P.; writing—original draft preparation, W.C.M.; writing—review and editing A.P., W.C.M. and R.D.; visualization, W.C.M.; funding acquisition, A.P. All authors have read and agreed to the published version of the manuscript.

**Funding:** This work has been carried out within the framework of the EUROfusion Consortium, funded by the European Union via the Euratom Research and Training Programme (grant agreement No. 101052200—EUROfusion). Views and opinions expressed are however those of the author(s) only and do not necessarily reflect those of the European Union or the European Commission. Neither the European Union nor the European Commission can be held responsible for them. AP also acknowledges, with thanks, the financial support provided by “Strengthening of the capacity of doctoral studies at the University of Latvia within the framework of the new doctoral model”, No. 8.2.2.0/20/I/006, and Scientific Research Project for Students and Young Researchers, Nr. SJZ/2021/5 implemented at the Institute of Solid State Physics, University of Latvia.

**Data Availability Statement:** The data presented in this study are available on request from the corresponding author. The data are not publicly available due to ongoing research.

**Conflicts of Interest:** The authors declare no conflict of interest.

## References

1. Ashfold, M.; Goss, J.; Green, B.; May, P.; Newton, M.; Peaker, C. Nitrogen in Diamond. *Chem. Rev.* **2020**, *120*, 5745. [PubMed]
2. Goss, J.P.; Briddon, P.R.; Jones, R.; Sque, S. Donor and acceptor states in diamond. *Diam. Rel. Mater.* **2004**, *13*, 684–690. [CrossRef]
3. Ferrari, A.; Saluto, S.; Gentile, F.; Mackrodt, W.; Dovesi, R. Substitutional nitrogen in diamond: A quantum mechanical investigation of the electronic and spectroscopic properties. *Carbon* **2018**, *134*, 354–365. [CrossRef]
4. Farrer, R. On the substitutional nitrogen donor in diamond. *Solid State Comm.* **1969**, *7*, 685–688.
5. Barklie, R.; Guven, J.  $^{13}C$  hyperfine structure and relaxation times of the P1 centre in diamond. *J. Phys. C Solid State Phys.* **1981**, *14*, 3621–3631. [CrossRef]
6. Cox, A.; Newton, M.; Baker, J.  $^{13}C$ ,  $^{14}N$  and  $^{15}N$  measurements on the single substitutional nitrogen centre (P1) in diamond. *J. Phys. Condens. Matter.* **1994**, *6*, 551. [CrossRef]
7. Zaitsev, A.M. *Optical Properties of Diamond—A Data Handbook*; Springer: Berlin/Heidelberg, Germany, 2001.
8. Hainschwang, T.; Fritsch, E.; Massi, L.; Rondeau, B.; Notari, F. The C centre isolated nitrogen-related infra-red absorption at  $2688\text{ cm}^{-1}$ : Perfect harmony in diamond. *J. Appl. Spectr.* **2012**, *79*, 737–743. [CrossRef]
9. Chrenko, R.; Strong, H.; Tuft, R. Dispersed paramagnetic nitrogen content of large laboratory diamonds. *Philos. Mag.* **1971**, *23*, 313–315. [CrossRef]
10. Walker, J. Optical absorption and luminescence in diamond. *Rep. Prog. Phys.* **1979**, *42*, 1605–1654. [CrossRef]
11. de Carvalho Nazare, M.H.; das Neves, A.J. Paramagnetic Nitrogen in diamond: Ultraviolet absorption. *J. Phys. C Solid State Phys.* **1987**, *20*, 2713.
12. Khan, R.U.; Martineau, P.M.; Cann, B.L.; Newton, M.E.; Twitchen, D.J. Charge transfer effects, thermo and photochromism in single crystal CVD synthetic diamond. *J. Phys. Condens. Matter* **2009**, *21*, 364214. [CrossRef]
13. Jones, R.; Goss, J.P.; Briddon, P.R. Acceptor level of nitrogen in diamond and the 270-nm absorption band. *Phys. Rev. B* **2009**, *80*, 033205. [CrossRef]

14. Tallaire, A.; Collins, A.T.; Charles, D.; Achard, J.; Sussmann, R.; Gicquel, A.; Newton, M.E.; Edmonds, A.M.; Cruddace, R.J. Characterisation of high-quality diamond grown by CVD with a low nitrogen addition. *Diam. Relat. Mater.* **2006**, *15*, 1700–1707. [[CrossRef](#)]
15. Iakoubovskii, K.; Adriaenssens, G.J. Optical transitions at substitutional nitrogen centre in diamond. *J. Phys. Condens. Matter* **2000**, *12*, L77–L81. [[CrossRef](#)]
16. Dovesi, R.; Saunders, V.R.; Roetti, C.; Orlando, R.; Zicovich-Wilson, C.M.; Pascale, F.; Civalleri, B.; Doll, K.; Harrison, N.M.; Bush, I.J.; et al. CRYSTAL17 User's Manual, Università di Torino. 2017. Available online: <http://www.crystal.unito.it> (accessed on 1 February 2023).
17. Dovesi, R.; Erba, A.; Orlando, R.; Zicovich-Wilson, C.M.; Civalleri, B.; Maschio, L.; Rérat, M.; Casassa, S.; Baima, J.; Salustro, S. Quantum-Mechanical Condensed Matter Simulations with CRYSTAL. *Wires* **2018**, *8*, e1360. [[CrossRef](#)]
18. Dovesi, R.; Pascale, F.; Civalleri, B.; Doll, K.; Harrison, N.; Bush, I.; D'Arco, P.; Noel, Y.; Rérat, M.; Carbonnière, P.; et al. The CRYSTAL code, 1976–2020 and beyond, a long story. *J. Chem. Phys.* **2020**, *152*, 204111. [[CrossRef](#)]
19. Mackrodt, W.; Salustro, S.; Civarelli, B.; Dovesi, R. Low energy excitations in NiO based on a direct  $\Delta$ -SCF approach. *J. Phys. Condens. Matter* **2018**, *30*, 495901–495915. [[CrossRef](#)]
20. Mackrodt, W.; Rérat, M.; Gentile, F.; Dovesi, R. An all-electron study of the low-lying excited states and optical constants of  $\alpha$ -Al<sub>2</sub>O<sub>3</sub> in the range 5–80 eV. *J. Phys. Condens. Matter* **2019**, *32*, 085901. [[CrossRef](#)]
21. Mackrodt, W.; Gentile, F.; Dovesi, R. The calculated energies and charge and spin distributions of the excited GR1 state in diamond. *J. Chem. Phys.* **2022**, *156*, 044708. [[CrossRef](#)]
22. WMackrodt, C.; Platonenko, A.; Dovesi, R. Self-trapped excitons in diamond: A  $\Delta$ -SCF approach. *J. Chem. Phys.* **2022**, *157*, 084707. [[CrossRef](#)]
23. Colasuonno, F.; Gentile, F.; Mackrodt, W.; Ferrari, A.; Platonenko, A.; Dovesi, R. Interstitial defects in diamond: A quantum mechanical simulation of their EPR constants and vibrational spectra. *J. Chem. Phys.* **2020**, *153*, 024119–024130. [[CrossRef](#)] [[PubMed](#)]
24. Becke, A. Density-functional exchange-energy approximation with correct asymptotic behavior. *Phys. Rev.* **1988**, *38*, 3098. [[CrossRef](#)] [[PubMed](#)]
25. Becker, A.D. Correlation energy of an inhomogeneous gas: A coordinate-space model. *J. Chem. Phys.* **1988**, *88*, 1053. [[CrossRef](#)]
26. Muscat, J.; Wander, A.; Harrison, N. On the prediction of band gaps from Hybrid functional theory. *Chem. Phys. Lett.* **2001**, *342*, 397–401. [[CrossRef](#)]
27. Adamo, C.; Barone, V. Toward reliable density functional methods without Adjustable parameters: The PBE0 model. *J. Chem. Phys.* **1999**, *110*, 6158. [[CrossRef](#)]
28. Perdew, J.P.; Burke, K.; Ernzerhof, M. Generalised Gradient Approximation Made Simple. *Phys. Rev. Lett.* **1996**, *77*, 3865. [[CrossRef](#)] [[PubMed](#)]
29. Perdew, J.P.; Yue, W. Accurate and simple density functional for the electronic exchange energy: Generalized gradient approximation. *Phys. Rev.* **1986**, *33*, 880.
30. Pascale, F.; D'Arco, P.; Dovesi, R. The ferromagnetic and anti-ferromagnetic phases (cubic, tetragonal, orthorhombic) of KMnF<sub>3</sub>. A quantum mechanical investigation. *Phys. Chem. Chem. Phys.* **2021**, *23*, 26780–26792. [[CrossRef](#)]
31. Cardona, M.; Thewalt, M.L. Isotope effects on the optical spectra of semiconductors. *Rev. Mod. Phys.* **2005**, *77*, 1173. [[CrossRef](#)]

**Disclaimer/Publisher's Note:** The statements, opinions and data contained in all publications are solely those of the individual author(s) and contributor(s) and not of MDPI and/or the editor(s). MDPI and/or the editor(s) disclaim responsibility for any injury to people or property resulting from any ideas, methods, instructions or products referred to in the content.